

Remote Sensing of Environmental Insults with Characteristic Spectral Features

Dr. Robert K. Vincent
Department of Geology
Bowling Green State University
Bowling Green, Ohio
rvincen@bgsu.edu

ABSTRACT

When it becomes desirable to employ multispectral remote sensing to map a particular environmental insult that is known or suspected to have occurred, it is useful to determine what spectral features are characteristic of the element or chemical compound comprising the environmental insult. This can be done in two general ways: by creating a quantitative algorithm via statistical methods that translates spectral band inputs of a particular remote sensing sensor into content of the element sought or by creating an enhancement image that displays the chemical compound of interest as red (or other color of choice), and almost everything else as other colors. The latter is not quantitative, but can often be helpful even when the quantitative algorithm approach fails. For both of these methods, spectral ratios (that have been dark-object-subtracted for atmospheric haze correction and sensor electronic offset in the case of the remote sensor data) are employed. Spectral ratios are more robust than single band information, not only for muting brightness variations caused by slope variations in the imaged scene, but also because they are most comparable to spectral ratios of laboratory reflectance spectra that have been averaged over the spectral bands of the remote sensor employed for the mapping. An example will be made for the environmental insult of phosphorous, which is important for both reducing the amount of fertilizers applied to agricultural fields and for controlling cyanobacteria algal blooms (which are sometimes toxic to animals and humans) in nearby lakes and streams.

INTRODUCTION

We live in exciting times. Not only is the planetary climate changing, but also the human species has proved to be perhaps only the second or third living species (behind cyanobacteria and perhaps dinosaurs) capable of changing the planet with their living habits. As we invent ever more chemical compounds with which to insult (change) our planetary environment, humans have finally become aware that insulting pollutants must be monitored. To do this well, monitoring will require remote sensing methods that measure areas of the Earth's surface, not just point measurements made by in situ instruments, which will remain useful, but cannot be the total answer. What is now happening in remote sensing of environmental insults mirrors what happened three decades ago when the AVHRR sensor, NOAA's precursor to the current MODIS sensor, first began monitoring sea surface temperature (SST) with space-borne thermal infrared sensors. Prior to AVHRR, SST was estimated from ocean buoy and ship thermometers that

would collect about 15,000 measurements of SST per year over all the oceans. Once AVHRR was orbited, it measured millions of pixels per frame, or many billions of pixels over all the oceans per year. Each pixel (1,000 m x 1,000 m in area) was a separate measurement, and for the first time, this detail in SST and SST anomalies (SSTA) permitted us not only to begin understanding the nature and causes of decadal weather patterns, such as El Nino, but also to discern that the best ocean fishing areas were where warm and cold water bodies met. Additionally, the cost savings of satellite remote sensing over in situ methods was well documented for SST measurements. Environmental monitoring is now following a similar path. We could never afford monitoring with in situ sensors alone, but with LANDSAT TM pixel sizes of 30 m x 30 m (a measurement every one-fifth of an acre), we can monitor practically every drinking water reservoir on the planet for toxic algal blooms (Vincent et al, 2004).

The remainder of this paper will be divided into four parts: library of laboratory and field spectra, translation of data to a robust parameter space, finding characteristic spectral features of target materials, and summary/conclusions.

LIBRARY OF LABORATORY AND FIELD SPECTRA

For multispectral and hyperspectral remote sensing, it all begins with laboratory and field spectra of materials that you wish to target for mapping, plus spectra of other materials that are found at the Earth's surface. In geology, those materials are usually minerals, but often also include soils, rocks, and vegetation (including lichen). It is always wise to know what the target material spectrum can be misidentified as, and that is where a library of spectra from Earth surface materials becomes vital. A USGS web site (<http://speclab.cr.usgs.gov/spectral-lib.html>) contains many reflectance spectra of minerals, plus a few vegetation spectra, that can serve as part of the spectral library. The researcher can add field or lab spectra to this library in the 0.35-2.5 micrometer range of the ASD field-portable spectrometer. Likewise, spectral emittance spectra can be calculated for 57 minerals from reflectance spectra (subtracted from 1.0 to yield emittance spectra) given by Salisbury et al. (1991) for the thermal infrared (TIR) wavelength region from approximately 2-15 micrometers.

TRANSLATION OF LIBRARY SPECTRA TO A ROBUST PARAMETER SPACE

The greatest control on brightness of objects on the Earth's surface is surface topography, which can have little to do with mineral or rock composition. Think of a conical hill illuminated by the sun in a SE position, which reflects more light from its SE-facing slope than from other directions around the hill. When the time of day or season moves the sun to the S, it is the S-facing slope that is brightest. These changes in illumination have little to do with surface composition, and can change from one time of day or one season to another. Thus, brightness changes from pixel to pixel in any one spectral band are common, but spurious to our intentions of mapping surface composition, and brightness values are not considered to be robust. It is helpful to translate average reflectance for each spectral band of the sensor of interest in the library spectra to a robust parameter, such as a spectral ratio, R_{ij} , which is a ratio of reflectances in the i th spectral band divided by the j th spectral band. Spectral ratios from a multispectral or

hyperspectral imager correlate well with spectra ratios from library spectra if the imager spectral bands are corrected for atmospheric haze and electronic offset of the sensor (Vincent, 1972 and 1997) by a method called dark object subtraction (DOS). A histogram of each single band is searched for the darkest digital number present in the image data set (which can be different for different spectral bands) and the additive haze/offset (dark object) is taken to be one digit less than that. When this dark object is subtracted from all pixels in the scene for that spectral band, the band is said to be dark-object-corrected, and the remaining variation in illumination is due to seasonal variations (if LANDSAT and ASTER are the sensors, because they are in sun-synchronous orbits, such that it is always the same local solar time on each overpass). Though a multiplicative constant still exists in the sensor data after it is dark-object subtracted, a ratio image made from such data that is contrast stretched to best display the dynamic range of the data acts to neutralize that multiplicative constant. Thus, dark-object-subtracted spectral ratios from sensor data have a behavior similar to spectral ratios of a library of mineral spectra, and library spectra can be used to determine which spectral ratios would display a given mineral as high (bright) or low (dark) in a spectral ratio of the sensor data for that mineral. More will be said about this point in the next section.

FINDING CHARACTERISTIC SPECTRAL FEATURES OF TARGET MATERIALS

In class I have asked my students how they would describe me to people meeting my airplane if I had a 1-inch purple mole in the middle of my forehead. They laugh and say that they would tell them to look for the only person on the airplane with a purple mole in the middle of the forehead, and I congratulate them for not giving out too much information. For instance, what if they also said that my weight was 183 lbs and that my hair was a mixture of black and gray? Someone meeting me that considered all of those three traits equally might actually miss identifying me because they thought I looked about 5 lbs heavier than that, or that my hair was gray enough to be considered gray, rather than a mixture of black and gray. The purple mole would be a characteristic feature of far greater uniqueness than weight or hair color.

The same is true of spectral features of target materials. Employing the entire reflectance spectrum of a material can actually yield higher errors of recognition than if we were sufficiently circumspect to use only the characteristic features of a spectrum, especially if all parts of the spectrum are weighted equally. (Try it if you don't believe me.) Employing uncharacteristic (non-unique) parts of the spectrum also requires more data processing time, data storage, and greater number of spectral bands than characteristic features would require. This begs a very important, but often understated question: How do you identify characteristic spectral features of any given material? I am going to give two very different types of examples, though both use only spectral ratios (corrected by dark object subtraction) as input parameters, not single bands, because of the greater robustness of the former. If LANDSAT TM data and ASTER data are reliably reduced to spectral reflectance from digital numbers (DN), that would improve the value of single band inputs, but my experience has been that the models employed to do that are not as trustworthy as empirical corrections, such as dark object subtraction.

The first type of my methods for finding characteristic features is called the spectral ratio code method, which will now be described for the ASTER sensor. ASTER has 14 different spectral bands, 3 in the VNIR (Visible/Near Infrared), 6 in the SWIR (Short-Wave Infrared), and 5 in the TIR (thermal infrared) spectral region. The number of non-reciprocal (if R_{ij} is used, R_{ji} is excluded) spectral ratios that can be produced by n spectral bands is equal to $n*(n-1)/2$. For the VNIR and SWIR spectral bands, $n=9$ and the number of non-reciprocal spectral ratios is $9*(8)/2=36$. Likewise, for the 5 TIR spectral bands, there are an additional 10 non-reciprocal spectral ratios possible. (TIR spectral bands are not mixed with VNIR or SWIR bands in a single spectral ratio because the former are all from emitted heat energy from the ground and the latter are all reflected sunlight from the ground; however, the spectral ratios of the two groups can be used together because the ratios are “apples to apples”.) Perry and Vincent (2009) have calculated 46 ASTER spectral ratios from spectra of over 500 minerals and some vegetation. Each spectral ratio was divided into deciles (10% of the spectra in the library) and given a ratio code of 9 for the highest decile, 8 for the second highest, down to 0 for the lowest decile. For each reflectance spectrum, a 46-digit ratio code (one digit between 9 and 0 for each spectral ratio) can be used to describe the spectrum. If you wish to display a particular mineral or target material as red in a 3-color visible image, you can do so by selecting a spectral ratio with a ratio code of 9 to display in red, and selecting two spectral ratios with a ratio code of 0 to display in green, and blue. The scene for that color ratio image is then stretched from 1%-99% as dark to bright, such that the target material, if present, will be displayed as red and almost all other materials will be displayed as colors other than red. In this scheme, each target material is displayed as red, but the spectral ratios are different for each material (or spectrum). If there are look-alikes (errors of commission), it is possible to figure out which few materials look like the target material in that color ratio image by looking for the same (or very similar) ratio codes for those three spectral ratios used to make the color ratio image. One high spectral ratio and two low spectral ratios (extremes) are assumed to be characteristic spectral features that are displayed as visible colors of red, green, and blue, respectively. For some target materials, there are multiple choices of spectral ratios that have 9 and 0 ratio codes, and you can experiment among them to see which does the best job of displaying the target material. For others materials, there may be no spectral ratios with 9 or 0 ratio codes, and 8 and 1 ratio code spectral ratios may have to be used. Characteristic spectral features are easier to find with more spectral ratios available from the sensor for which the ratio codes are calculated.

An example is given in Figure 1, taken from Perry and Vincent (2009) for a region in the Big Horn Mountains of Wyoming. The top image of Figure 2 shows the color ratio image of $R(12,11)$, $R(5,4)$, and $R(9,8)$ displayed as RGB, respectively, for a small region near the town of Kaycee, Wyoming. ASTER spectral bands 1-3 are in the VNIR wavelength region, bands 4-9 are in the SWIR region, and bands 10-14 are in the TIR region. For the gypsum laboratory spectrum, $R(12,11)$, $R(5,4)$, and $R(9,8)$ have ratio codes of 9, 0, and 0, respectively, such that gypsum is displayed as red in the color ratio image at the top of Figure 1. In the bottom image of Figure 1, gypsum outcrops are gray to white in color in the field. This color ratio image does very well in recognizing gypsum and nothing else in the scene because it employs three extreme ratios (characteristic spectral features) that are very distinctive for gypsum.

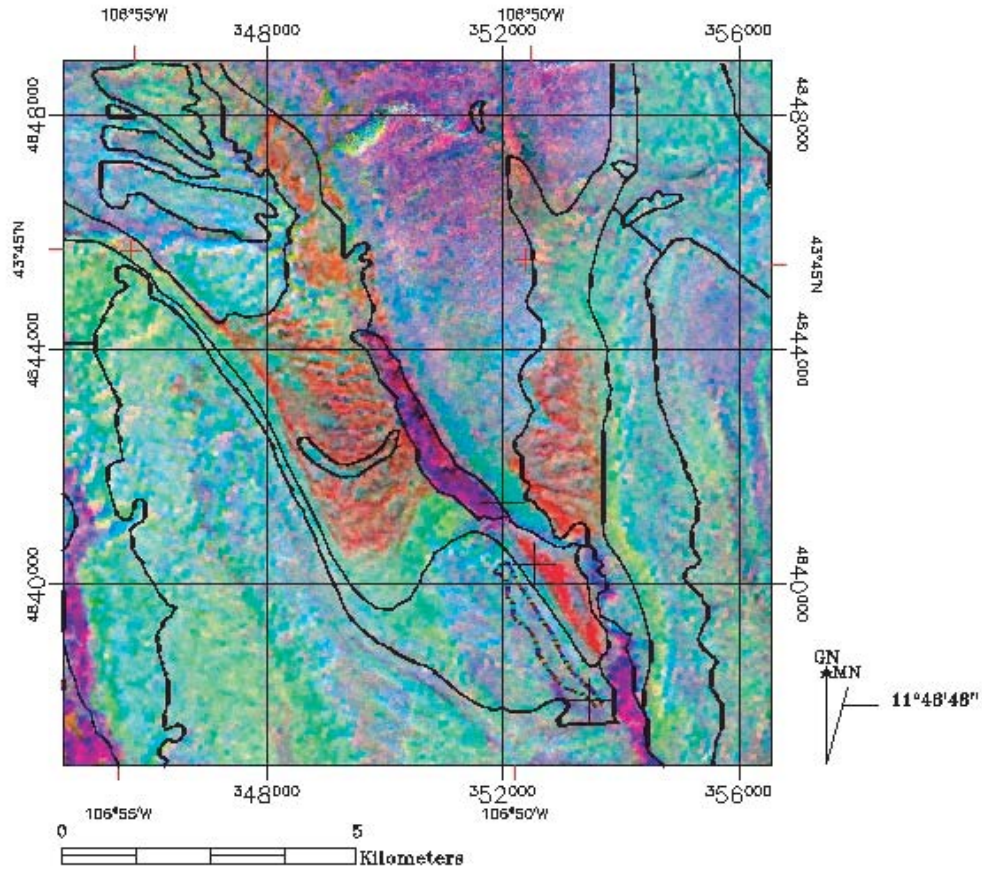


FIG. 1. Top: Color ratio image of R(12,11), R(5,4), and R(9,8) displayed as RGB, respectively, for a small region within the Kaycee subset image. Red regions in this image are supposed to be gypsum. The cross-hair in the red area is where Powder River basin (PRB) sample PRB6 was collected. Bottom: Color field photo of the sample PRB6 collection site, a gypsum outcrop. (From Perry and Vincent, 2009)

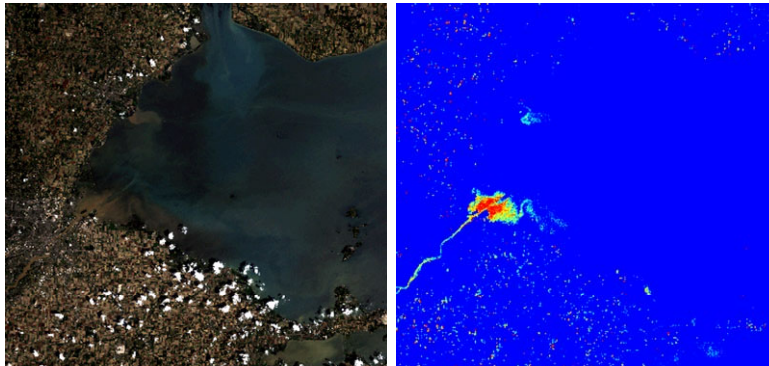
The second type of method that I have used to determine characteristic spectral features is to statistically create a model, or algorithm, that is designed to map the content of a single element or compound that the target material is known to contain, assuming that the content is uniform over the pixel size of the sensor. The algorithm itself is the characteristic spectral feature, and it is quantitative because it maps amounts of a single element or compound in the material of interest. An example of the quantitative algorithm method is provided in a paper by Vincent et al (2004), where an algorithm (now patented by Bowling Green State University and licensed to Blue Water Satellite, Inc., a new company in Bowling Green, OH) was created that maps the content of phycocyanin, the characteristic pigment that makes cyanobacteria blue-green in color, using only LANDSAT TM spectral ratios as inputs. The procedure, explained in greater detail in the paper, involved collection of 30 water samples from a fast boat in the Western Basin of Lake Erie, collected about 1 mile apart, within approximately 1.5 hours of satellite overpass. A GPS device was used to determine the site of each sample collection site. A terrain-corrected data set of LANDSAT TM data for that overpass (on July 1, 2000) was employed to extract the digital numbers at those 30 sample collection sites for each of the six 30-m resolution LANDSAT TM bands (1-5 and 7). Phycocyanin content was measured in the laboratory for each water sample by a fluorometer, resulting in values of phycocyanin content (PC) in units of $\mu\text{g/L}$, or parts per billion (ppb), assuming that PC and water have similar specific gravities and that 1 liter of water contains 1,000 g of PC. Using Minitab as the statistical software, the top two subsets of one-ratio algorithms, two-ratio algorithms, down to 15-ratio algorithms were saved, and the others were ignored. The statistical parameter $R^2(\text{Adj.})$ first rises, then falls as more spectral ratios are added to the algorithms, because the statistics are being overdriven. The algorithm that had the highest $R^2(\text{Adj.})$ and also did not fail the Durbin-Watson Test for self-correlation of the input parameters (all of which were spectral ratios of LANDSAT TM data) was selected as the best PC algorithm for LANDSAT TM data, as follows:

$$\text{PC}(\mu\text{g/L})=47.7-9.21*\text{R31}+29.7*\text{R41}-118*\text{R43}-6.81*\text{R53}+41.9*\text{R73}-14.7*\text{R74} \quad (\text{Eqn. 1})$$

where PC is phycocyanin content and R_{ij} is the dark-object-corrected spectral ratio of average reflectance in the i th and j th LANDSAT TM bands, respectively, for a pixel. The $R^2(\text{Adj.})$ for this model was 77.6%.

PC was calculated from Eqn. 1 for each pixel and the results are imaged in the ERMAPPER software package as a color pseudo image, yielding the right image of Figure 2. The root mean square (rms) error of PC calculated from the LANDSAT 7 overpass model (July 1, 2000) was 3.1 $\mu\text{g/L}$ for each value of PC measured in a LANDSAT 5 overpass (September 27, 2000) water sample data set, or about 26% of the total range in PC for the later date. Later work has shown that the PC algorithm in Eqn. 1 has an effective working range of 3-17 ppb (or $\mu\text{g/L}$), where the lower limit is taken to be the approximate rms error in PC on the withheld data set.

Figure 2. LANDSAT TM View of Western Basin of Lake Erie on July 1, 2000: Natural Color Image (Left); PC Low-Bloom Image Stretched from 0 (Blue) to 10 (Red) ppb of Phycocyanin (Right). Bloom is dominated by *Microcystis*.



There were some surprises in this result. First, as was pointed out in the Vincent et al (2004) paper, LANDSAT TM bands 2 (520– 600 nm) and 3 (630–690 nm) have a gap in coverage where phycocyanin has most of its absorption band (maximum absorption is approximately at 620 nm), yet this rigorous statistical method had calculated the $R^2(\text{Adj.})$ for every possible combination of 15 spectral ratios, from 1-ratio to 15-ratio algorithms, and this algorithm in Equation 1 had risen to the top, in a procedure somewhat akin to a biological evolutionary process: survival of the fittest. It had also yielded reasonable results on a withheld data set on another LANDSAT overpass date. Second, the longer wavelength bands of LANDSAT TM, bands 4-5 and 7, were important in the winning algorithm, and their penetration capability in water is realized to be much lower than the penetration of the visible bands (numbers 1-3). Neither of these surprises is comforting to optical physicists, especially those that think they can model everything accurately with a physical model. How can you possibly map phycocyanin when most of the phycocyanin absorption band is in a spectral gap not covered by any spectral band of the satellite sensor employed for this experiment? Why would the least water-penetrating of the spectral bands be so prominent in the resulting PC algorithm? Couldn't you come up with an algorithm for any element or compound that would appear to work?

Starting from the end and working backwards, I quickly found that the answer to the last question was a resounding “No” by trying the same procedure on many different elements and compounds for which I could obtain data. As for the importance of bands 4, 5, and 7, we were looking at cyanobacteria, which can change their buoyancy to match environmental conditions (greater buoyancy in still waters on bright days). Perhaps the longer wavelength band inclusions to Equation 1 helps the algorithm tell when things are at or near the surface or not, and this may be important for cyanobacteria, that can range in depth from several meters to the surface. Other algae may stay at the surface most of their lives. The first question was seemingly a more difficult conundrum. The hardest thing to let go of was the idea that if the strongest absorption

band of the material for which you are searching is outside the spectral coverage of your sensor, you shouldn't be able to image that material with that sensor. Optical modeling might help our understanding, except for the fact that some cyanobacteria form colonies in the shape of spheres of all sizes, such as *microcystis*, and others are filamentous and form colonies of myriads of shapes and sizes make it obvious that physical models that could show how cyanobacteria blooms reflect light at many wavelengths would be very complex. Also, the data on how those sizes and shapes changed with growth do not exist to the level required by Mie scattering, or other such optical models. On the plus side, the math was rigorous in testing of all spectral ratio combination possibilities, and most of those combinations failed to even make the final list of 30 (the top two algorithms each for 1, 2, 3, ...and 15 spectral ratio combinations). Also, the $R^2(\text{Adj.})$ was 77.6%, for the top algorithm, and it worked on a withheld data set. The pluses outweighed the minuses, and I decided to go with "Darwinian" math and to use the algorithm in Eqn. 1 for mapping emergent blooms of cyanobacteria in lakes and streams with LANDSAT TM data.

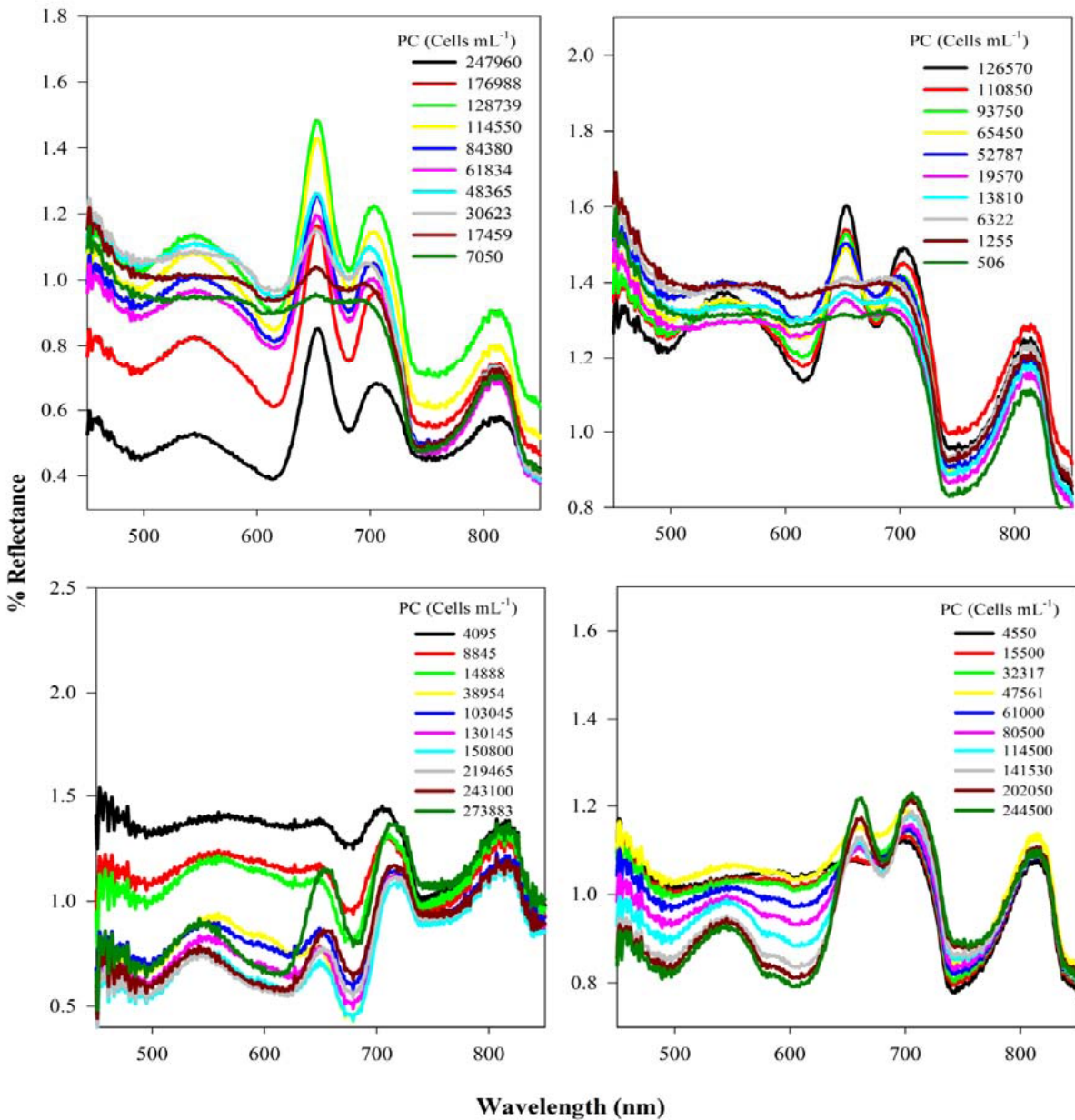
It was a good choice, because Misrah et al (2009) have since shown with their excellent laboratory spectroscopic experiment of two different strains of lab-cultured cyanobacteria and one strain of green algae that wavelength regions outside the major absorption features can provide higher correlation than spectral data from within those absorption bands with phycocyanin content. In particular, they showed for cyanobacteria strains *Synechocystis* and *Anabaena* how an absorption band (reflection minimum in the VNIR spectrum) for phycocyanin at 620 nm and for chlorophyll *a* at 680 nm causes a reflectance maximum to appear at 654 nm, the latter of which is well inside the wavelength range of LANDSAT TM band 3 (630–690 nm). They noted that this reflectance maximum, though not an absorption band for either phycocyanin or chlorophyll *a*, increases with increasing concentration of phycocyanin. Figure 3 shows reflectance spectra that demonstrate this spectral behavior, with different chlorophyll *a* contents (Chl *a*) present for each graph as stated in the figure caption. The authors went on to suggest that a ratio of the reflectance at 700 nm to the reflectance at 600 nm would be highly correlated with phycocyanin content, based purely on their laboratory data, with little influence from chlorophyll *a* content. Neither of these wavelengths is in an absorption minimum of either phycocyanin or chlorophyll *a*. It is likely that when they start using ratios of satellite data to map lakes and streams, even if the satellite contains narrow spectral bands around these two wavelengths, they will find that PC can be better mapped with multiple spectral ratios than with this one alone. Their laboratory work did not extend to wavelengths higher than 850 nm, which is well short of LANDSAT TM bands 5 and 7.

More recently, Sridhar et al (2009) created a quantitative algorithm that is a characteristic spectral feature of total phosphorous in bare soil. Algorithms for several metals and nutrients were sought, using the same methodology applied to the phycocyanin algorithm (Vincent et al, 2004). The best of these was an algorithm for total phosphorous on land (TPL) as given below:

$$\text{TPL}(\text{mg/kg, or ppm})= 4156-1690 *R51+2257* R73 \quad \text{Eqn. 2}$$

where R51 is the spectral ratio of LANDSAT TM band 5 to band 1 and R73 is the spectral ratio of LANDSAT TM band 7 to band 3, after dark object subtraction. The $R^2(\text{Adj.})=67.9\%$ and the standard error was 531.2 ppm. Two agricultural fields near Oregon, Ohio, to which known tons

Figure 3. Percent reflectance spectra of *Synechocystis* (all but lower right graph) and *Anabaena* (lower right graph) blooms grown in the laboratory and showing the appearance and dynamics of a 654 nm peak in reflectance for different Chl-*a* concentrations of 3.40 $\mu\text{g/L}$ and 2.48 $\mu\text{g/L}$, respectively, for the upper left and upper right graphs, and 13.32 $\mu\text{g/L}$ for the lower left graph. No Chl-*a* values were given for the *Anabaena* bloom in the lower right graph. (taken from Misrah et al, 2009). Phycocyanin and Chl-*a* are both produced by cyanobacteria.



per acre of biosolids (sewage sludge) had been applied, were sampled in 70 locations (3 depths at each location), and the resulting elemental analysis for P and several other elements were measured by an induced coupled polarization optical emission spectrometer (ICP-OES). Figure 4 shows the averaged spectra for soil samples from 3 different depths (0, 30, and 50 cm below the surface) of each of the two fields to which biosolids had been applied for 17 years. The average phosphorous content is shown for the two separate fields in different columns and from the three depths (highest values of P at the surface) of samples in three rows.

Figures 5 and 6 show the correlation between predicted (from Eqn. 2) and actual TPL and an image of the predicted TPL over the two fields on May 20, 2005, the day after the biosolids were last applied. Figures 7 and 8 show the same (using the May 20, 2005 TPL model of Eqn. 2) for June 5, 2005.

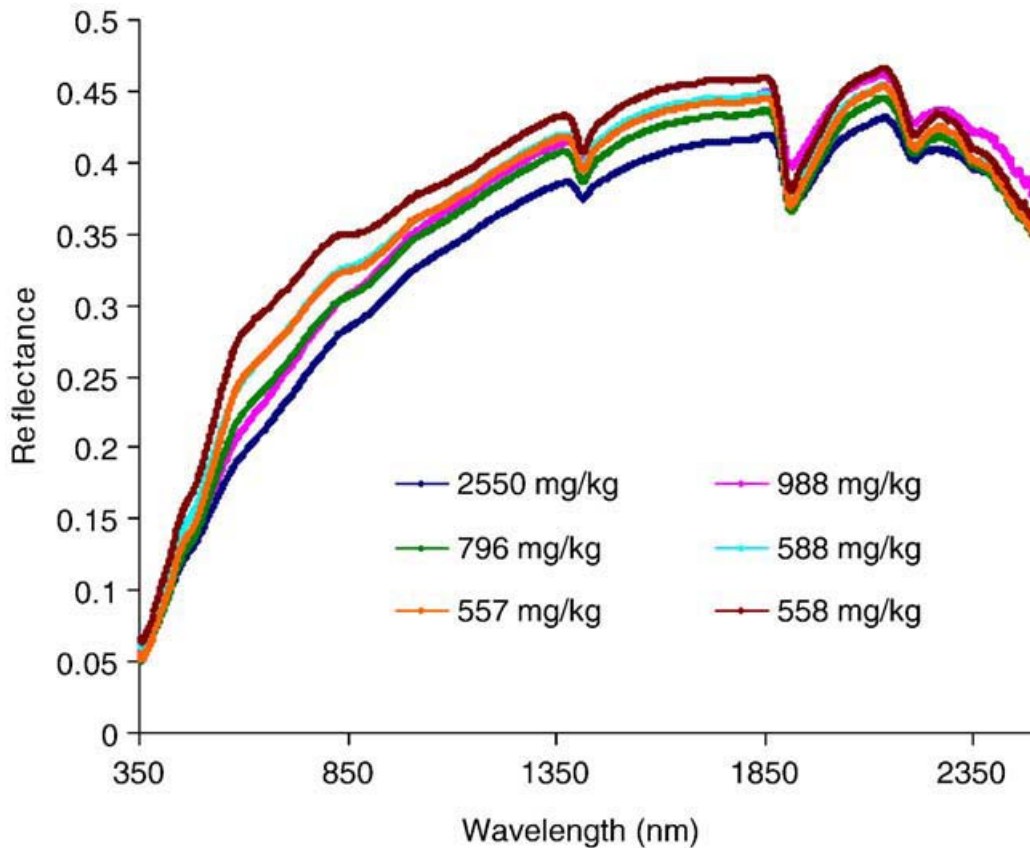


Figure 4. Averaged (n=35) spectral reflectance of the soil samples collected at 0, 30 and 50 cm depths in F34 (left column) and F11 (right column) treated fields. Also given are the averaged total P concentrations (in mg/kg) corresponding to the soil samples. The spectral reflectance of the soils decreases with increase in P concentration. The surface soil samples of field F34 have high P concentration (2550 mg/kg) and low spectral reflectance throughout the spectral range, compared to the rest of the soil samples. (Taken from Sridhar et al, 2009)

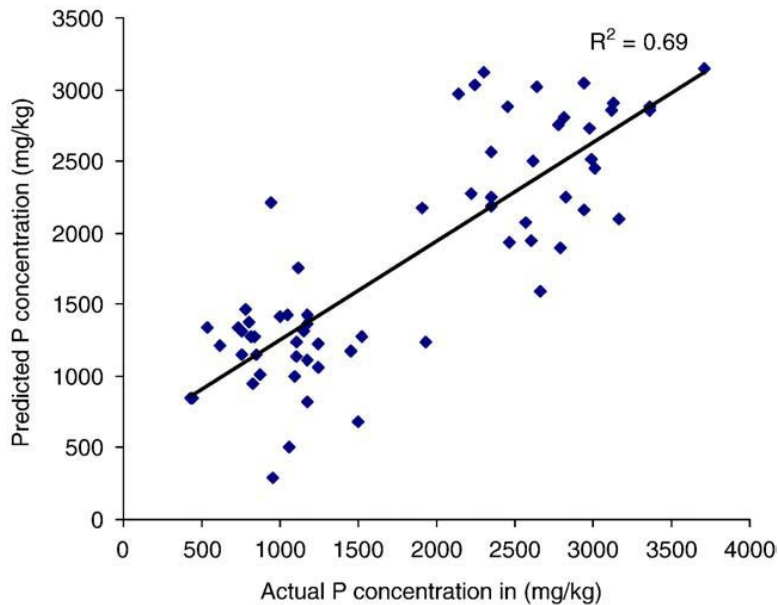


Figure 5. Actual versus predicted P concentration (in mg/kg) of surface soil samples using the dark object subtracted best P spectral ratio model being applied to the LANDSAT 5 TM frame of May 20, 2005, which was also used for developing the model. (Taken from Sridhar et al, 2009)

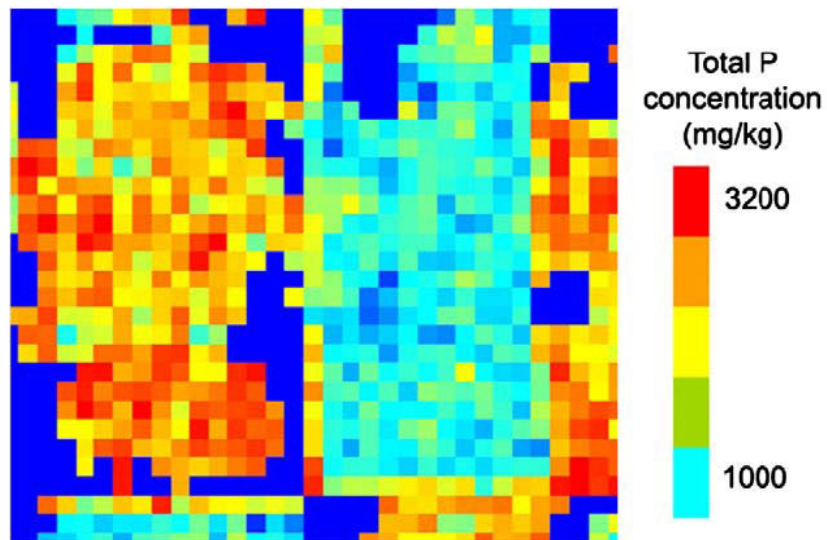


Figure 6. Image showing the total P concentration (mg/kg) in surface soil samples of fields F34 (left side of the image) and F11 (right side of the image), displayed as red (high P content) to turquoise (low P content), obtained by applying the best P spectral ratio model to the LANDSAT 5 TM frame of May 20, 2005, which was also used for developing the model. Dark blue pixels are non-bare soils with vegetation on them. (Taken from Sridhar et al, 2009)

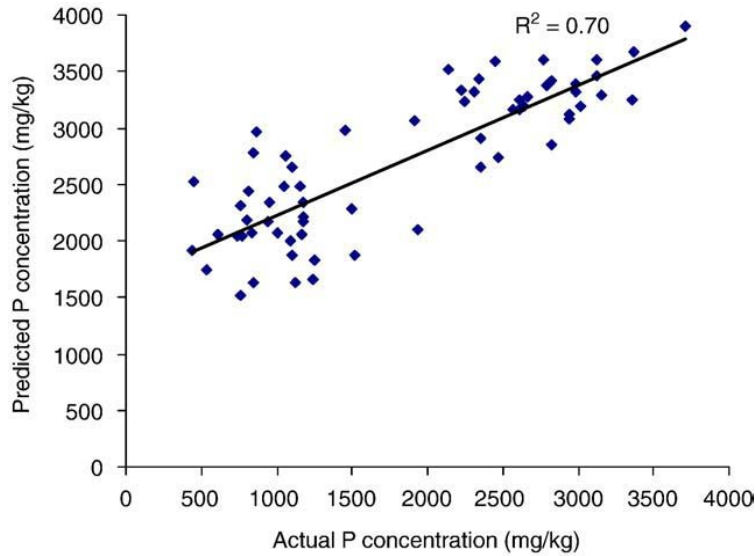


Figure 7. Actual versus predicted P concentration (in mg/kg) of surface soil samples using the dark object subtracted best P spectral ratio model being applied to the LANDSAT 5 TM frame of June 5, 2005. (Taken from Sridhar et al, 2009)

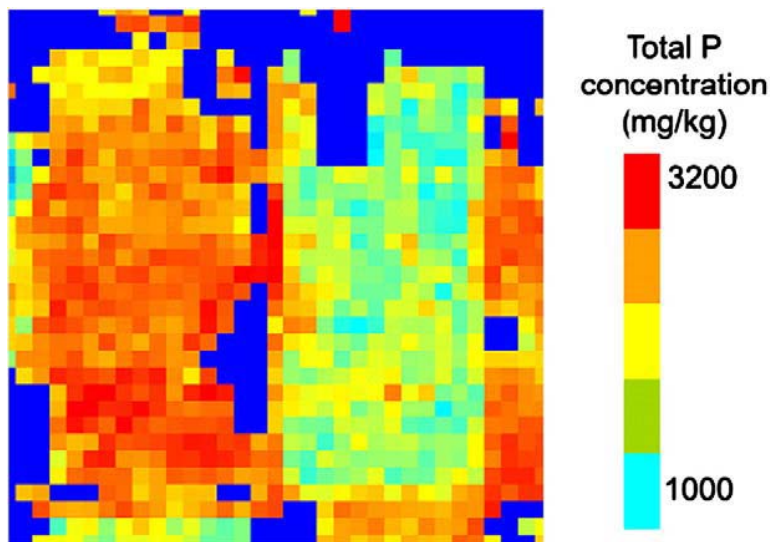


Figure 8. Image showing the total P concentration (mg/kg) in surface soil samples of fields F34 (left side of the image) and F11 (right side of the image), displayed as red (high P content) to turquoise (low P content), obtained by applying the P spectral ratio model to the LANDSAT 5 TM frame of June 5, 2005. Dark blue pixels are non-bare soils with vegetation on them. (Taken from Sridhar et al, 2009)

These results show that the results for the two overpasses were similar, indicating robustness for the model. The soil samples were collected only once, a day before the earlier of the two dates. Another test was performed using this same TPL model on the now-famous Tennessee fly (coal) ash spill of Dec. 22, 2008. Figure 9 shows images 32 days before, 9 hours after, and 40 days after the spill. The TPL model shows the high-P fly ash in its containment, spread after the spill, and mediated with sawdust and seeds during those 3 times. Both the TPL and copper models from the previous paper functioned reasonably well on all three dates, though the ground data were not available in suitable form to make possible a quantitative comparison between predicted and actual P values.

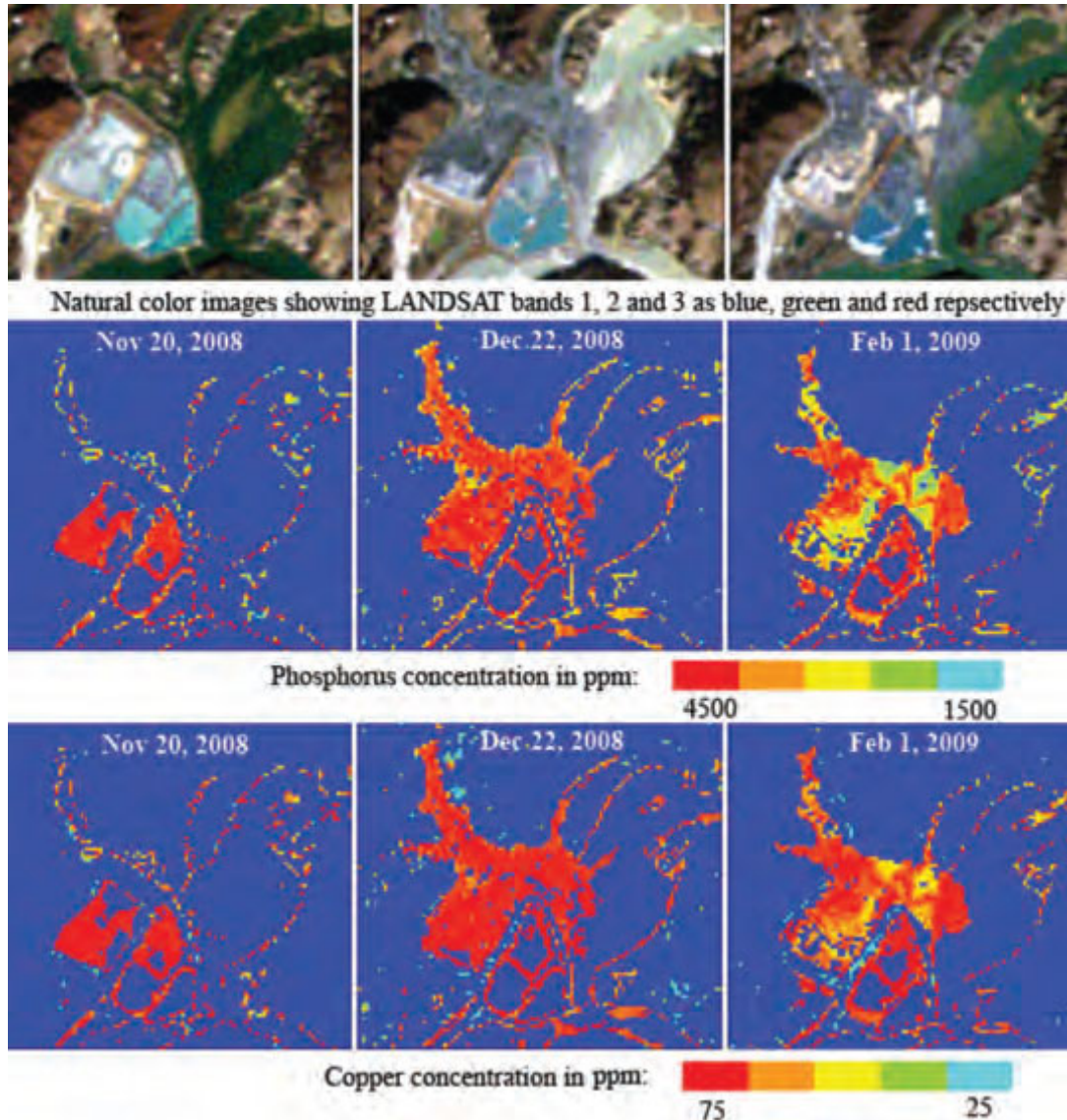


Figure 9. The LANDSAT TM images of the Tennessee fly ash spill area acquired on November 20, 2008 (32 days before fly ash spill); December 22, 2008 (9 hours after fly ash spill) and February 1, 2009 (40 days after fly ash spill), respectively. The images in rows 1-3 represent the natural color image, surface P concentration image, and surface Cu concentration image, respectively. Dark blue regions are not bare soils. (Taken from Sridhar and Vincent, 2009)

SUMMARY AND CONCLUSIONS

It is important to build a library of spectra representative of typical materials found at the Earth's surface, including minerals, rocks, some vegetation, and materials of special interest to the researcher because you have to understand the spectral properties of both the background (represented by library of spectra) and the target material to find those wavelengths at which the target material is contrasted (stands out) from the background. In fact, increasing contrast between target and background is probably the most important task in multispectral remote sensing. Part of building a spectral library is solved by owning a good field-portable spectrometer and learning how to use it well.

It is also important to translate all spectra into a robust set of spectral parameters, so that whatever algorithms you design for finding a given material will have the greatest chance of being useful under a variety of illumination and atmospheric conditions. An algorithm that works only under a few narrow conditions is far less useful than one that is robust enough to be useful under a variety of environmental conditions. This is especially important for algorithms constructed to monitor living vegetation, which requires sensor platform overpasses under many different illumination and atmospheric conditions. Dark-object-subtracted spectral ratios offer an example of robust spectral parameters. Others include use of satellite data reduced to spectral reflectance, if the owner of the data provides such data that is consistently extracted from the sensor with high accuracy.

Finally, it is important to limit your search to the characteristic spectral features of a target material that make it stand out from other materials. Including spectral features that do not lend uniqueness to the "signature" of a target material can lead to false alarms, inefficient processing times, and higher costs of searching for that material. Although characteristic spectral features often include contrasting absorption bands (usually reflectance minima in the VNIR and SWIR) with adjacent spectral regions, they can occur completely outside absorption bands of a target material. For the same material, characteristic spectral features can be very different from one sensor to another.

I have described two types of characteristic spectral features: spectral ratio codes and quantitative algorithms that consist of weighted combinations of spectral ratios. The former is an enhancement tool that creates color ratio images in which the target material appears red (if present in the imaged scene) by assigning a spectral ratio for which the target material has a very high value to the red display color, and assigning two spectral ratios which have very low values for that material to the green and blue display colors. The latter is an algorithm that maps the content of a particular element or compound in a restricted class of surface features, such as in water or in bare soil, and the algorithm itself becomes the characteristic spectral feature. It is created and tested by statistical methods. When these quantitative algorithms are employed, they should be tested on a withheld data set before they are employed and after further use, the limits of the algorithm should be determined, because an algorithm should not be expected to operate outside the range of input element or compound contents that were used in creation of the algorithm. However, sometimes the usefulness of the algorithm may extend beyond that range. In general, mapping a given element or compound over an extensive range of content will require two or three algorithms for different content ranges of that same element or compound.

In this paper I have reviewed two quantitative algorithms, one for phycocyanin content of low cyanobacteria blooms and the other a total phosphate content of bare soil. There are others that I have created, also, but the number of successful algorithms is far outnumbered by the number of elements and compounds for which no good algorithm was found, after extensive testing with LANDSAT TM data. With more spectral bands, the number of successful algorithms will increase. I expect that successful quantitative algorithms will increase rapidly, even for LANDSAT TM data, in the next several years. We have hardly begun to plumb the depths of what can be done with LANDSAT TM data, after 27 years of that sensor being in orbit, much less the newer sensors (ASTER and HYPERION) and the sensors yet to be orbited. Multispectral and hyperspectral remote sensing has quite an interesting future ahead.

ACKNOWLEDGEMENTS

This research was partly funded by NOAA Grant NA07OAR4170502 and Blue Water Satellite, Inc., Bowling Green, Ohio.

REFERENCES

Mishra, Sachidananda, Deepak R. Mishra, and Wendy M. Schluchter, 2009, A Novel Algorithm for Predicting Phycocyanin Concentrations in Cyanobacteria: A Proximal Hyperspectral Remote Sensing Approach, Remote Sensing, Vol. 1, pp 758-775 (ISSN 2072-4292, www.mdpi.com/journal/remotesensing).

Perry, Jason L., and R. K. Vincent, 2009, ASTER Brightness and Ratio Codes for Minerals: Application to Lithologic Mapping In West-Central Powder River Basin, Wyoming, Reviews in Economic Geology, v. 16, Remote Sensing and Spectral Geology, Society of Economic Geologists.

Salisbury, J.S., Walter, L.S., Nergo, N., and D'Aria, D.M., 1991, Infrared (2.1–15 μ m) spectra of minerals: Baltimore, Johns Hopkins University, 267p.

Sridhar, B. B. Maruthi, Robert K. Vincent, Jason D. Witter and Alison L. Spongeberg, 2009, Mapping Total Phosphorus Concentration of Surface Soils With LANDSAT TM Data, Science of the Total Environment, Vol. 407, No. 8, pp. 2894-2899.

Sridhar, B.B. Maruthi and Robert K. Vincent, 2009, Mapping and Estimation of Phosphorus and Copper Concentrations in Fly Ash Spill Area using LANDSAT TM Images, Photogrammetric Engineering and Remote Sensing, September Issue, pp. 1031-1033.

Vincent, R.K., 1972, An ERTS Multispectral Scanner Experiment for Mapping Iron Compounds, Proceedings of the Eighth International Symposium on Remote Sensing of Environment, Ann Arbor, Michigan, Vol. II, pp. 1239-1247.

Vincent, R.K., 1997, Fundamentals of Geological and Environmental Remote Sensing, Prentice Hall, Upper Saddle River, New Jersey, 400 pp.

Vincent, R.K., X. Qin, R. M. L. McKay, J. Miner, K. Czajkowski, J. Savino, and T. Bridgeman, 2004, Phycocyanin Detection from LANDSAT TM Data for Mapping Cyanobacterial Blooms in Lake Erie, Remote Sensing of Environment, Vol. 89, No. 3, pp 381-392.